Acta Cryst. (1989). B**45**, 78–85

Structure of Putrescinium Dinitrate at Three Low Temperatures (30, 120 and 275 K)*

BY MARIUSZ JASKÓLSKI

Department of Crystallography, Faculty of Chemistry, A. Mickiewicz University, ul. Grunwaldzka 6, 60-780 *Poznań, Poland*

AND IVAR OLOVSSON

Institute of Chemistry, University of Uppsala, Box 531, *S*-75121 *Uppsala, Sweden*

(*Received* 8 *March* 1988; *accepted* 2 *September* 1988)

Dedicated to Professor Maciej Wiewiórowski on the occasion of his 70th birthday

Abstract

The X-ray structure of putrescinium dinitrate (1,4-butanediammonium dinitrate, $C_4H_{14}N_2^{2+}.2NO_3^-$, M_r = 214·2) has been studied by X-ray diffraction at 30, 120 and 275 K and compared with the structure previously determined at room temperature (291 K). In this range of temperatures the crystals are triclinic, $P\bar{1}$, with $Z = 2$. The unit-cell parameters at 30 K are: $a = 8{\cdot}5478$ (4), $b = 5{\cdot}4927$ (2), $c = 10{\cdot}2563$ (5) Å, $\alpha = 91{\cdot}664$ (4), $\beta = 93{\cdot}572$ (3), $\gamma = 103{\cdot}337$ (4)°, $V = 467{\cdot}17$ (4) Å^3, $R = 0{\cdot}034$ for 2490 observed reflexions. The unit cell contains two centrosymmetric putrescinium dications located on two different inversion centers. Cation I has the extended all-*trans* conformation while cation II is in a partly folded *gauche*$^+$–*trans*–*gauche*$^-$ conformation. Cation II exists in the structure in two disordered *gauche*$^+$–*trans*–*gauche*$^-$ alternatives (*A* and *B*) located on a single inversion center and sharing common terminal C–NH_3^+ groups. The N–C–C–C torsion angle in form II*B* deviates by 15·3 (3)° from the ideal *gauche* conformation (60°) over the whole range of temperatures. The analogous torsion angle in form II*A* assumes a more favorable value at the lowest temperatures [−67·5 (1)° at 30 K] but shows increasing deviations from the ideal *gauche* conformation as the temperature rises, the situation at room temperature being similar to that present in II*B*. The amount of form II*A* decreases at a growing rate with temperature and is 80·1 (4)% at 30 K, 78·9 (4)% at 120 K and 74·0 (8)% at 275 K. The temperature dependence of the unit-cell constants suggests that a phase transition is possible slightly above 300 K in agreement with the temperature variation of the II*A* : II*B* ratio. The II*A* → II*B* transformation does not involve the H-bond donor and acceptor groups and therefore the H-bond network remains unchanged even at the lowest temperatures. The anisotropic temperature factors vary regularly with temperature. The vibrations of the nitrate O atoms show high anisotropy even at the lowest temperatures and increase more rapidly with temperature than those of the remaining atoms.

Introduction

Putrescine (1,4-butanediamine) is a linear biogenic diamine present in all prokaryotic and eukaryotic cells. This very simple molecule is an important factor in various biological processes, its stabilizing effect on the conformation of nucleic acids being perhaps most important. In biological systems putrescine exists in diprotonated form and a number of structural studies of the conformational properties of the putrescinium dication in crystals with various anions have been published. With only one exception, the putrescinium dication was found at a crystallographic inversion center. In putrescinium hydrogen phosphate dihydrate (Jaskólski, Alejska & Wiewiórowski, 1986) the putrescinium dication is not located on an inversion center but even in that case it assumed a symmetric conformation with a non-crystallographic inversion center. This tendency to be highly symmetric is combined with conformational flexibility, as in some structures the putrescinium dication exists in the extended all-*trans* conformation (putrescinium dichloride, Chandrasekhar & Pattabhi, 1980; putrescinium hydrogen phosphate dihydrate, Jaskólski, Alejska & Wiewiórowski, 1986), while in others it is in a partly folded *gauche*$^+$–*trans*–*gauche*$^-$ (g^+tg^-) form [putrescinium bis(diethylphosphate), Furberg & Solbakk, 1972; putrescinium diphosphate, Takusagawa & Koetzle, 1978, 1979; Woo, Seeman & Rich, 1979]. Furberg & Solbakk (1972) reported that the dication in putrescinium bis(diethylphosphate) is disordered and assumes two different g^+tg^- forms located on a single

* Studies of Biogenic Polyamines. V. Part IV: Bartoszak & Jaskólski (1988).

0108-7681/89/010078-08$03.00

inversion center. The two forms share common C—N$^+$ termini but their central C—C bridges are different and cross at the inversion center. Furberg & Solbakk did not determine the proportion of the two alternative forms of the dication, but refined the structures assuming 0·5 occupancies for each.

Recently, the room-temperature (291 K) structure of putrescinium dinitrate has been reported (Jaskólski, 1987) and it turned out to be a fascinating illustration of all the results obtained in the previous studies summarized above. The peculiarity of putrescinium dinitrate consists in the fact that all the tendencies and properties of the putrescinium dication which previously have been delineated from many structures can be observed in one single structure: (i) the structure contains two *centrosymmetric* dications located on two inversion centers; (ii) one of the dications is all-*trans*, the other g^+tg^-; (iii) the g^+tg^- cation is *disordered* and exists in two alternative conformations (with common C—N$^+$ groups) similar to those reported by Furberg & Solbakk. However, the refinement of the putrescinium dinitrate structure also included the site occupation factor for the disordered fragment which converged at 73(2)% for alternative *A* and 27 (2)% for alternative *B* (Jaskólski, 1987). It was not possible at that stage to decide the character of the disorder and to find out on what factors the *A* : *B* ratio could possibly depend. Another intriguing problem was whether the increase of reflexion intensities with X-ray exposure reported for putrescinium dinitrate at room temperature (Jaskólski, 1987) could be related to any structural changes involving the *A* and *B* alternatives of the disordered dication. Consequently, we decided to investigate the structure of putrescinium dinitrate at several temperatures below room temperature.

It should be noted that the putrescinium dication was studied using low-temperature diffraction techniques by Takusagawa & Koetzle who reported on the neutron structure (1978) and on the charge density (1979) of putrescine diphosphate at 85 K.

Experimental

A crystal of approximate dimensions 0·3 × 0·3 × 0·35 mm was studied with Mo $K\alpha$ radiation using a four-circle diffractometer with 400 mm χ-circle (Huber) equipped with a two-stage closed-cycle helium low-temperature attachment (Aracor) and controlled (from a MicroVAX II computer) by the Stoe *DIF*4 program system (revision 6·2A). The low-temperature device has a temperature sensor located on the cool finger and coupled with the temperature control system. Thus, the temperature set on the control unit corresponds to the temperature at the cool finger and is usually lower than that at the crystal site. The actual temperature at the crystal site has been calibrated by observing the phase transitions of KH_2PO_4 (122 K) and $KMnF_3$ (187 and 81 K). At the lowest temperatures (when almost no heating is required) and at the highest temperatures (when heating outweighs cooling) the discrepancy between those two temperatures is not very large, *ca* 5 K. In the medium range, however, it is estimated to be around 20 K. In this paper only the estimated temperatures at the crystal site are used except in Table 1, which also gives the temperature reading on the control unit.

Table 1. *Experimental details*

Estimated temp. at crystal site (K)	30±2	120±5	275±3
Temp. at cooler (K)	24·7±0·5	100·0±1·5	270·0±1·0
λ (Å)	0·71073	0·71073	0·71073
Total number of reflexions	3048	2876	3032
Number of unique reflexions	2715	2730	2836
R_{int}	0·0141	0·0173	0·0228
Check reflexion fluctuations (%)			
$\bar{1}\,0\,3$	−1·9, +1·9	−0·9, +1·6	−2·2, +1·4
$3\,\bar{1}\,4$	−3·0, +3·0	−2·7, +3·4	−5·4, +3·2
$1\,2\,3$	−3·4, +4·0	−3·8, +3·6	−3·1, +4·4
Determination of intensities from profiles	LL*	BPB†	BPB†
Observed reflexions $I \geq 1{\cdot}96\sigma(I)$	2490	2357	2052
Final least-squares refinement			
Function minimized	$\sum w(F_o-F_c)^2$		
Weights‡	$k_1/(\sigma^2F + k_2 \times 10^{-5}F^2)$		
k_1	2·93	0·25	1·00
k_2	4	1	11
Excluded reflexions	113, 500	—	—
Number of parameters	204	204	204
Number of constraints	17	21	21
R	0·034	0·036	0·054
wR	0·041	0·041	0·050
S	5·04	1·20	2·50
Max. Δ/σ	0·07	0·02	0·005
Final ΔF map			
Max. $\Delta\rho$ (e Å^{-3})	0·43§	0·38	0·25
Min. $\Delta\rho$ (e Å^{-3})	−0·37	−0·29	−0·36

* Lehmann & Larsen (1974) algorithm using the program by Lundgren (1982).

† Background–peak–background method using the Stoe data collection program and assuming a constant number of steps for each background.

‡ k_2 selected to give optimum error distribution in weight analysis, k_1 estimated by least squares (Sheldrick, 1976).

§ All peaks higher than 0·28 e Å^{-3} were located between covalently bonded atoms and could be interpreted as bonding electrons.

The measurements were carried out at temperatures of 30, 275 and 120 K (in that order). The orientation matrix was calculated by a least-squares fit of the setting angles of 18 carefully centered reflexions ($9 < 2\theta < 25°$). For unit-cell parameters determination 43 reflexions with $14{\cdot}7 < 2\theta < 30{\cdot}9°$ were used. Their accurate 2θ values were obtained by centering each reflexion at positive and negative 2θ and ω and taking $\omega(+) - \omega(-)$ as the true 2θ value. Unit-cell parameters and their estimated standard deviations are given in Table 2.

Intensity measurements were carried out using θ:2θ scans in the range $2 \leq 2\theta \leq 60°$ (max. $\sin\theta/\lambda = 0{\cdot}7035$ Å^{-1}) for $-12 \leq h \leq 12$, $-7 \leq k \leq 7$, $0 \leq l \leq 14$. The scan range in 2θ was 2·2–2·6° plus $\alpha_1 - \alpha_2$ split and the scan rate (2θ) varied from 1·2 to 7·2° min^{-1}, the target $I/\sigma(I)$ being 50. Three standard reflexions monitored every 2 h were used to check the

Table 2. *Crystallographic data*

$C_4H_{14}N_2^{2+}.2NO_3^-$, $M_r = 214{\cdot}2$, triclinic, $P\bar{1}$, $Z = 2$, $F(000) = 228$.

Temperature (K)	30	120	275
a (Å)	8·5478 (4)	8·5482 (4)	8·5513 (4)
b (Å)	5·4927 (2)	5·4982 (2)	5·5086 (2)
c (Å)	10·2563 (5)	10·3193 (5)	10·5079 (5)
α (°)	91·664 (4)	91·726 (4)	91·310 (4)
β (°)	93·572 (3)	93·259 (3)	92·586 (3)
γ (°)	103·337 (4)	103·127 (3)	102·376 (3)
V (Å^3)	467·17 (4)	471·10 (4)	482·72 (4)
D_x (g cm^{-3})	1·522	1·510	1·473
μ (Mo $K\alpha$) (cm^{-1})	0·96	0·95	0·93

Table 3. *Geometrical restraints used in the refinements*

30 K	C(22)–C(23*B*)	1·540 (1) Å
	C–H for H atoms with partial occupancies	1·08 (1) Å
	H···H between geminal H atoms of form *B*	1·74 (2) Å
	N–H	1·02 (1) Å
120 K	As for 30 K plus	
	C(22)···H(233)	
	···H(234)	
	C(23*B*)···H(223)	
	H(224)	2·16 (1) Å
275 K	As for 120 K	

stability of the measurements. Their intensity fluctuations did not show any regularities and were within acceptable limits (Table 1). To further check the quality of the data, more than the unique sphere was measured in each data collection and some regions of the reciprocal lattice were collected twice. The absorption effect was negligible (*cf.* Table 2). Other experimental details are summmarized in Table 1.

The refinements started from the room-temperature parameters (Jaskólski, 1987). All non-H atoms were refined with anisotropic temperature factors, all H atoms with isotropic temperature factors. For the ordered H atoms individual U_{iso} were refined while for those with partial occupancies [at C(22), C(23*A*), C(23*B*)] only one thermal parameter was refined for each group of atoms attached to a common C atom. In the refinement some restraints were applied to the geometry of the disordered fragment of cation II (Table 3). The disordered CH_2 groups were restrained to tetrahedral geometry with standard C–H distances and the C(22)–C(23*B*) bond distance was restrained to 1·540 (1) Å since unrestrained refinement yielded systematically too large values [*e.g.* 1·596 (4) Å at 30 K]. The ammonium N–H distances were also restrained as they were systematically too short [around 0·88 (1) Å] when unrestrained. The refinements included the occupancy factor (k) of the disordered atoms of cation II*A*, with the occupancy of the corresponding atoms of II*B* calculated as $k' = 1 - k$. To check if the model was reasonable, additional least-squares refinements were run in which the k and k' parameters were varied independently. The results confirm that the model is consistent since the sums $k + k'$ obtained in this way were 1·000 (6) (30 K), 1·008 (7) (120 K) and 0·982 (11) (275 K). An attempt to refine the empirical isotropic extinction parameter yielded an insignificantly small value and therefore no extinction correction was applied.

All calculations were performed using *SHELX*76 (Sheldrick, 1976) as well as programs described by Lundgren (1982) and by Jaskólski (1982). Thermal-ellipsoid illustrations were drawn using *ORTEP*II (Johnson, 1976) and the space-filling model was generated with *PLUTO* (Motherwell & Clegg, 1978). Atomic scattering factors were from *International Tables for X-ray Crystallography* (1974).

Results and discussion

Table 4 reports the final positional and thermal parameters at 30, 120 and 275 K.* The development of thermal motion of the atoms with temperature is illustrated in terms of thermal ellipsoids in Fig. 1. In general, only the size of the ellipsoids changes with temperature whereas their shapes and orientations remain the same. The exception is the disordered fragment of cation II (Fig. 1*b*), but this is not unusual as the anisotropic temperature factor is probably not an adequate model here. It is interesting to note that the relatively large amplitude of thermal motion of the nitrate ions is also present at the lowest temperatures and manifests itself with highly anisotropic thermal ellipsoids of the O atoms. In Fig. 2 the diagonal components of the anisotropic temperature factors are plotted *versus* temperature. The regular behavior of these plots in the range 30–275 K is a convincing test of the quality of the results. The irregularities in the range 275–291 K are most certainly due to the lower quality of the room-temperature data (Jaskólski, 1987). Fig. 2 illustrates that the thermal motion of the nitrate O atoms is not only larger than that of the remaining atoms but that is also increases more rapidly with temperature. The high thermal motion observed for C(22) in cation II is not unusual as this atom is directly connected to the disordered fragment [C(23*A*,*B*)] and may itself show some disorder which would be then absorbed by its temperature factor.

Fig. 3 shows the site occupation factor k of the alternative *A* of the disordered cation II plotted *versus* temperature. The proportion of alternatives *A* and *B*, which at 30 K is 0·801 (4) : 0·199 (4), gradually decreases with temperature and at 291 K (Jaskólski, 1987) is 0·73 (2) : 0·27 (2). Even though the last point in Fig. 3 is of relatively lower precision, the general trend in this plot indicates that with increasing temperature cation II*A* is transformed into II*B*. At temperatures above 300 K the increase of the amount

* Lists of structure factors and H-atom parameters have been deposited with the British Library Document Supply Centre as Supplementary Publication No. SUP 51291 (45 pp.). Copies may be obtained through The Executive Secretary, International Union of Crystallography, 5 Abbey Square, Chester CH1 2HU, England.

Table 4. *Fractional coordinates* ($\times 10^4$) *and anisotropic thermal parameters* ($Å^2 \times 10^4$) *for non-*H *atoms*

The anisotropic temperature factor is of the form: $\exp[-2\pi^2(h^2a^{*2}U_{11} + \cdots + 2hka^*b^*U_{12})]$.

	x	y	z	U_{11}	U_{22}	U_{33}	U_{23}	U_{13}	U_{12}
30 K									
N(11)	2773 (1)	−2354 (2)	6159 (1)	74 (4)	90 (4)	81 (4)	13 (3)	4 (3)	29 (3)
C(12)	2053 (1)	−185 (2)	5826 (1)	70 (4)	68 (4)	91 (4)	12 (3)	−1 (3)	21 (3)
C(13)	375 (1)	−1104 (2)	5158 (1)	70 (4)	77 (4)	93 (4)	7 (3)	−11 (3)	16 (3)
N(21)	2489 (1)	822 (2)	1283 (1)	77 (4)	90 (4)	90 (4)	5 (3)	22 (3)	26 (3)
C(22)	3195 (1)	1628 (2)	19 (1)	126 (4)	150 (5)	87 (5)	47 (4)	47 (4)	88 (4)
C(23*A*)	4234 (1)	−101 (2)	−446 (1)	68 (6)	84 (6)	73 (6)	5 (4)	7 (4)	24 (4)
C(23*B*)	4963 (2)	1402 (9)	79 (5)	84 (23)	118 (25)	85 (24)	10 (19)	9 (18)	11 (18)
N(10)	4163 (1)	6086 (2)	3306 (1)	66 (3)	86 (4)	62 (4)	3 (3)	−6 (3)	11 (3)
O(11)	4214 (1)	8382 (1)	3449 (1)	105 (3)	60 (3)	131 (4)	8 (3)	2 (3)	12 (2)
O(12)	5049 (1)	5302 (1)	2549 (1)	95 (3)	151 (4)	102 (4)	−16 (3)	31 (3)	44 (3)
O(13)	3201 (1)	4544 (1)	3946 (1)	125 (3)	90 (3)	114 (4)	26 (3)	46 (3)	−11 (3)
N(20)	−77 (1)	5287 (2)	8343 (1)	89 (4)	88 (4)	54 (4)	6 (3)	−2 (3)	35 (3)
O(21)	418 (1)	7634 (1)	8308 (1)	110 (3)	69 (3)	137 (4)	29 (3)	29 (3)	17 (3)
O(22)	−1373 (1)	4412 (1)	8862 (1)	91 (3)	89 (3)	112 (3)	21 (3)	36 (3)	8 (2)
O(23)	709 (1)	3882 (1)	7852 (1)	148 (4)	143 (4)	107 (4)	−20 (3)	20 (3)	96 (3)
120 K									
N(11)	2783 (1)	−2319 (2)	6151 (1)	143 (4)	195 (5)	153 (5)	35 (4)	13 (4)	54 (4)
C(12)	2051 (1)	−166 (2)	5816 (1)	138 (5)	152 (5)	166 (5)	20 (4)	3 (4)	31 (4)
C(13)	380 (1)	−1094 (2)	5158 (1)	146 (5)	160 (5)	175 (5)	11 (4)	−18 (4)	27 (4)
N(21)	2485 (1)	827 (2)	1282 (1)	154 (4)	163 (5)	192 (5)	14 (4)	38 (4)	54 (4)
C(22)	3188 (1)	1608 (2)	21 (1)	219 (6)	239 (6)	179 (6)	63 (5)	52 (5)	123 (5)
C(23*A*)	4233 (2)	−123 (3)	−437 (1)	155 (7)	174 (8)	144 (7)	−5 (5)	17 (5)	47 (6)
C(23*B*)	4954 (3)	1376 (9)	73 (5)	163 (26)	144 (27)	131 (25)	21 (20)	17 (20)	21 (20)
N(10)	4164 (1)	6095 (2)	3305 (1)	149 (4)	164 (4)	139 (4)	9 (3)	−6 (3)	20 (3)
O(11)	4208 (1)	8385 (1)	3444 (1)	202 (4)	134 (4)	234 (5)	13 (3)	6 (3)	19 (3)
O(12)	5040 (1)	5307 (2)	2545 (1)	223 (4)	299 (5)	221 (5)	−30 (4)	51 (4)	98 (4)
O(13)	3216 (1)	4572 (2)	3948 (1)	331 (5)	183 (4)	252 (5)	54 (4)	110 (4)	−27 (4)
N(20)	−69 (1)	5258 (2)	8332 (1)	176 (4)	190 (5)	125 (4)	17 (4)	10 (4)	75 (4)
O(21)	422 (1)	7590 (2)	8291 (1)	207 (4)	169 (4)	288 (5)	65 (3)	59 (4)	27 (3)
O(22)	−1363 (1)	4401 (1)	8850 (1)	199 (4)	170 (4)	235 (4)	38 (3)	71 (3)	25 (3)
O(23)	716 (1)	3855 (2)	7847 (1)	325 (5)	330 (5)	231 (5)	−41 (4)	38 (4)	214 (4)
275 K									
N(11)	2816 (2)	−2248 (3)	6129 (1)	301 (8)	422 (9)	351 (9)	90 (7)	30 (7)	96 (7)
C(12)	2046 (2)	−138 (3)	5789 (2)	301 (9)	320 (9)	374 (10)	33 (8)	13 (8)	50 (7)
C(13)	402 (2)	−1067 (3)	5157 (2)	320 (9)	346 (9)	383 (10)	30 (8)	−30 (8)	55 (7)
N(21)	2494 (2)	865 (3)	1295 (2)	378 (9)	366 (9)	523 (11)	35 (8)	90 (8)	125 (7)
C(22)	3153 (2)	1547 (4)	33 (2)	490 (12)	477 (12)	442 (12)	74 (9)	73 (10)	230 (10)
C(23*A*)	4219 (3)	−205 (5)	−393 (3)	408 (16)	387 (18)	374 (15)	−38 (12)	40 (12)	83 (13)
C(23*B*)	4925 (4)	1356 (14)	59 (8)	405 (50)	269 (48)	425 (47)	65 (35)	128 (37)	88 (36)
N(10)	4180 (2)	6113 (3)	3297 (1)	350 (8)	334 (8)	359 (8)	25 (6)	−6 (7)	36 (6)
O(11)	4204 (2)	8382 (2)	3431 (1)	439 (8)	310 (7)	510 (8)	16 (6)	16 (6)	43 (6)
O(12)	5026 (2)	5333 (3)	2529 (1)	531 (9)	655 (10)	567 (10)	−71 (8)	139 (8)	227 (8)
O(13)	3273 (2)	4625 (3)	3952 (2)	856 (12)	434 (9)	629 (10)	158 (8)	270 (9)	−38 (8)
N(20)	−38 (2)	5177 (3)	8294 (1)	392 (8)	408 (9)	306 (8)	23 (6)	35 (7)	149 (7)
O(21)	440 (2)	7482 (3)	8242 (1)	494 (8)	400 (8)	660 (10)	148 (7)	147 (7)	29 (6)
O(22)	−1322 (2)	4361 (1)	8808 (1)	446 (8)	381 (8)	644 (10)	75 (7)	188 (7)	34 (6)
O(23)	746 (2)	3793 (3)	7826 (2)	734 (11)	748 (11)	625 (11)	−94 (9)	110 (9)	470 (10)

of II*B* may be very rapid and at higher temperatures the dominant form may be II*B* or the crystal possibly may be transformed into a structure containing exclusively cation II*B*. The regular variation of the $A : B$ ratio with temperature is most probably independent of the specimen used for measurement and of its history as Fig. 3 includes data obtained for two different crystals.

Another indication that the putrescinium dinitrate crystals could undergo a phase transition at temperatures above 300 K is provided in Fig. 4 which plots the relative changes of unit-cell constants with temperature. With increasing temperature a and b are practically constant while α, β and γ tend to 90°. At the same time c increases at a growing rate. The total effect is best illustrated by ΔV which shows a rapid increase at temperatures slightly above 300 K. Thus, the II*A*→II*B* transformation suggested by Fig. 3 is also manifested in a variation of unit-cell constants as indicated by Fig. 4. This transformation must be a dynamic and reversible process as the low-temperature measurements were performed in the order 30, 275, 120 K. The question, however, remains what is the mechanism of this transformation, what is the energy difference between forms II*A* and II*B* in the crystal and what energy is necessary for the transition II*A*→II*B*? The latter energy should not be very high as the transition II*A*→II*B* occurs even at the lowest temperatures but also it cannot be very low as the two forms of cation II are clearly distinguishable even at room temperature. As the two forms, II*A* and II*B*, have common C–NH_3^+ groups, the transition II*A*→II*B* involves only a displacement of the inner C–C bridge of the putrescinium skeleton. To estimate the internal barrier to such a transformation quantum-chemical or molecular-mechanical calculations will be necessary. To estimate the variation of the intermolecular interaction energy during this transition even more complicated calcula-

tions would be necessary. Fig. 5 represents a space-filling model of cation II*A* and suggests [particularly in combination with Fig. 2 of Jaskólski (1987)] that the two forms of cation II may have similar intermolecular interaction energies as the inner $-(CH_2)_4-$ part of the cation is very compact and occupies nearly the same space in both forms.

Analysis of molecular geometry at low temperatures and comparison with the results of the room-temperature study (Jaskólski, 1987) indicates a good consistency. The differences in bond distances which have any statistical significance can be in general attributed to errors due to thermal motion. Table 5 lists the geometrical data at 30, 120 and 275 K. Those at 30 K should be nearly free from thermal-motion errors but even at that temperature some effects have been observed when the uncorrected N—O bond distances in the nitrate groups [average 1·257 (4) Å] were compared with the values corrected for riding motion [average 1·262 (3) Å]. The riding-motion corrections seem to be systematically overestimated at higher temperatures, the average corrected N—O bond lengths at 120, 275 and 291 K being 1·263 (2), 1·268 (2) and 1·275 (2) Å, respectively. This may illustrate the increasing contribution from anharmonic effects but for 291 K (Jaskólski, 1987) is probably also due to extra errors contained in the temperature factors (Cu data, absorption neglected).

The conformation around the C(12)—C(13) bond in cation I is effectively constant in the whole range of temperatures, the N(11)—C(12)—C(13)—C(13′) torsion angles at 30, 120, 275 K (this work) and at 291 K (Jaskólski, 1987) being respectively 178·9 (1), 178·8 (1), 178·5 (2) and 178·6 (3)°. Similarly, no significant changes are observed for the N(21)—C(22)—C(23*B*)—C(23*B*′) angles [75·1 (3), 75·1 (3), 76·8 (5) and 74 (1)°]. The analogous angle in the II*A* alternative, however, shows a significant variation, the corresponding values being −67·5 (1), −68·1 (1), −70·7 (3) and −72·5 (4)°. Therefore, as the temperature is lowered this torsion angle is relieved from the strain (deviation from 60°) which at elevated temperatures approaches the strain which is present in the II*B* form over the whole range of temperatures. In view of the above discussion one can conclude that cooling the crystal to the lowest temperatures transforms cation II to the alternative *A* which becomes increasingly predominant and at the same time tends toward its most favorable conformation.

The N(10) nitrate anion is planar within experimental error in the whole range of temperatures, the respective χ^2 values being 4·34, 0·06, 1·95 and 2·02. The χ^2 values for the N(20)-nitrate plane indicate very significant non-planarity at low temperatures (40·31, 30·04, 21·07 and 1·89). This observation, however, is merely an illustration that the non-planarity of this

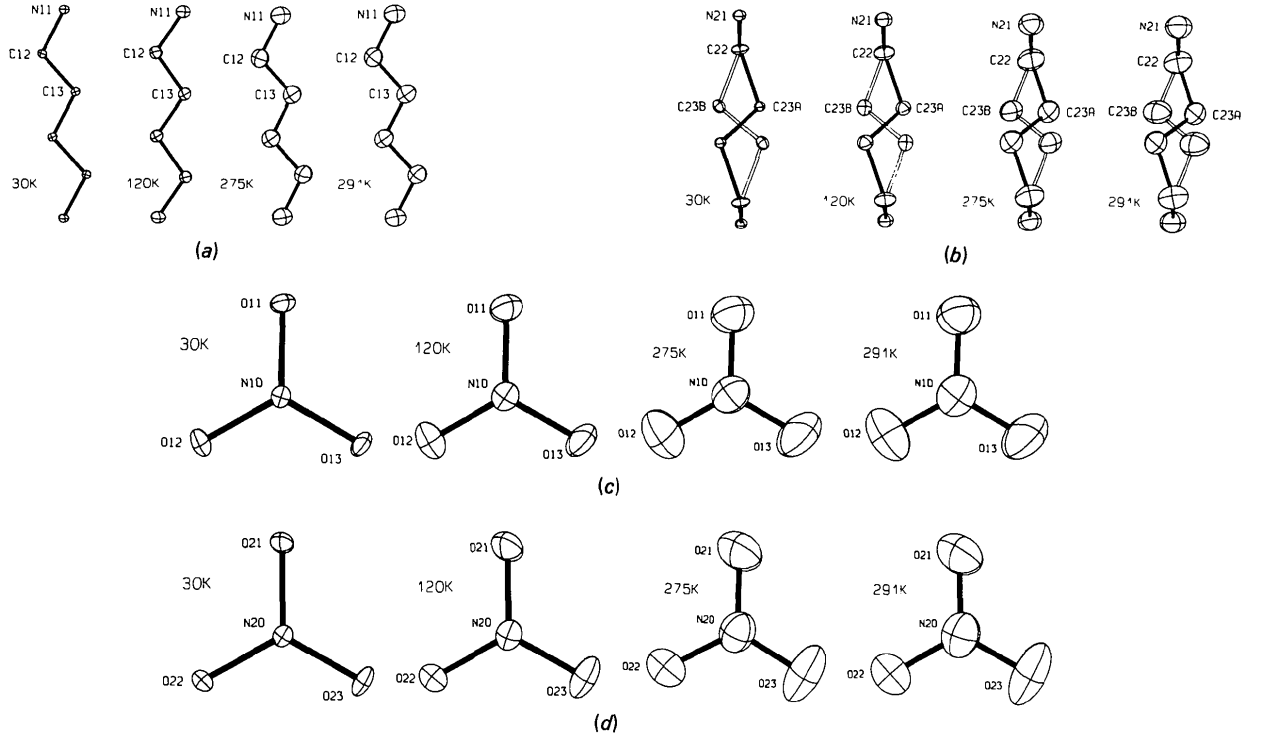

Fig. 1. Thermal-ellipsoid representation (50% probability level) of the ions at different temperatures [30, 120 and 275 K – this work, 291 K – taken from Jaskólski (1987)]: (*a*) cation I, (*b*) cation II, (*c*) N(10) nitrate, (*d*) N(20) nitrate.

group could only be detected using the best quality data as the deviations of N(20) from the O···O···O planes have nearly the same absolute magnitude at all temperatures [0·0059 (8), 0·0065 (10), 0·0072 (13), 0·005 (3) Å].

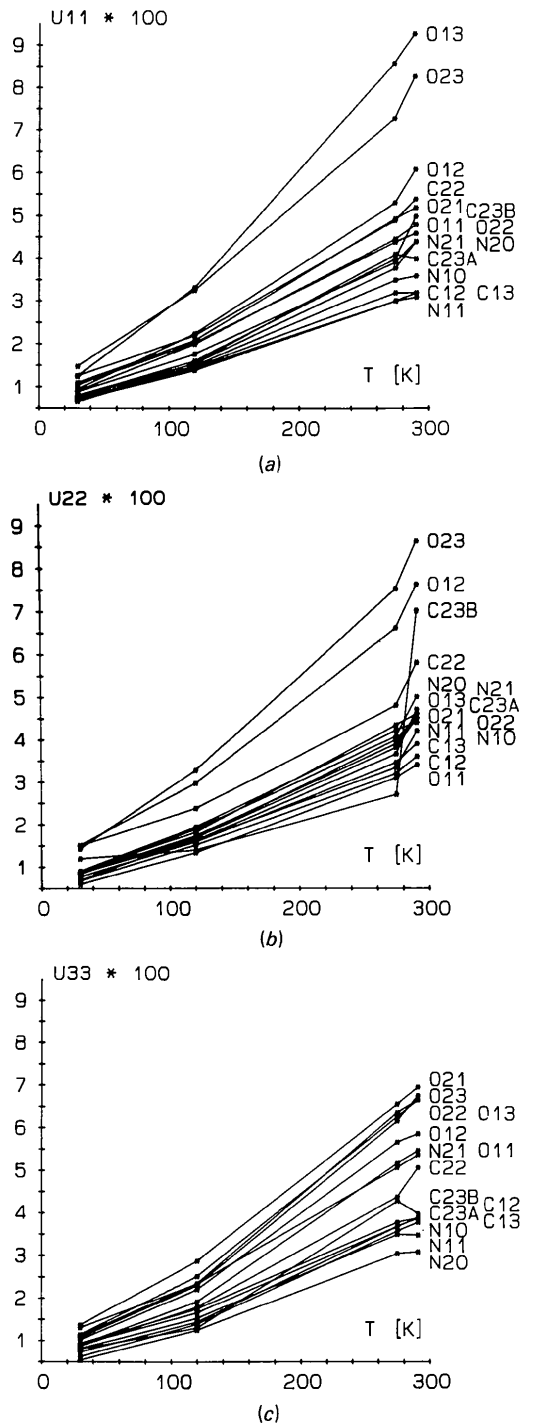

Fig. 2. Variation of the diagonal components of the anisotropic temperature factors with temperature: (*a*) U_{11}, (*b*) U_{22}, (*c*) U_{33}. The data for 291 K have been taken from Jaskólski (1987).

The general organization of the H-bond network remains unchanged in the structure in the investigated range of temperatures. This is not surprising as the H-bond acceptors (NO_3^- groups) and donors ($-NH_3^+$ groups) are not involved in the structural transformations described above. This last statement may not be quite true with reference to the $-N(21)H_3^+$ group which might assume different orientations in II*A* and II*B*. As described in the *Experimental* section, the positions and isotropic temperature factors of H(211), H(212) and H(213) were included in the least-squares refinements. The final $\Delta\rho$ maps did not indicate any alternative orientation of the $-N(21)H_3^+$ group but the behavior of the temperature factors of the H atoms at N(21) [particularly when compared with the corresponding values for N(11)] suggests that the $-N(21)H_3^+$ group is also in some way involved in the structural transformations. This is illustrated by the mean U_{iso} values for the H atoms at N(21) [N(11)] which at 30, 120 and 275 K (this work) and 291 K (Jaskólski, 1987) are 0·023 [0·021], 0·042 [0·032], 0·101 [0·064] and 0·150 [0·069] respectively. Table 6 shows the H-bond parameters at 30 K. They are slightly yet fairly systematically different from those reported for the room-temperature structure (Jaskólski, 1987). The general trend (which is observed throughout the investigated range of temperatures) is that with increasing temperature the shorter and nearly linear N–H··· O bonds become longer and more bent while the weaker and angular bonds tend to assume more favorable geometry.

Finally, it may be appropriate to go back to the problem of the unusual reflexion intensity variation observed during the measurements of putrescinium dinitrate at room temperature (Jaskólski, 1987). As mentioned in the *Experimental* section, in the present experiments no check intensity variations larger than those that could be explained by temperature instability have been observed. In this context the unusual intensity increase reported for the room-temperature experiment can be explained as resulting either from

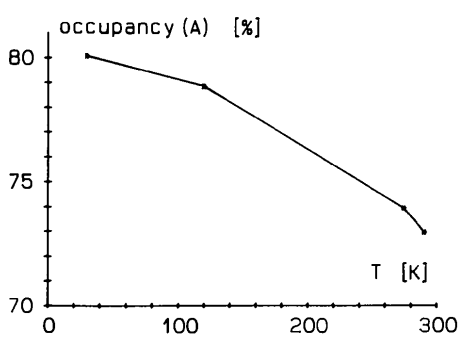

Fig. 3. Variation of the site occupation factor k of the alternative *A* of the disordered cation II with temperature. The point at 291 K has been taken from Jaskólski (1987).

changes in extinction of a fresh crystal or from the fact that the $A:B$ ratio at 291 K is very sensitive to temperature.

We hope that the studies of putrescinium dinitrate at elevated temperatures which are currently in progress will verify our present conclusions and will shed more light on this fascinating structure.

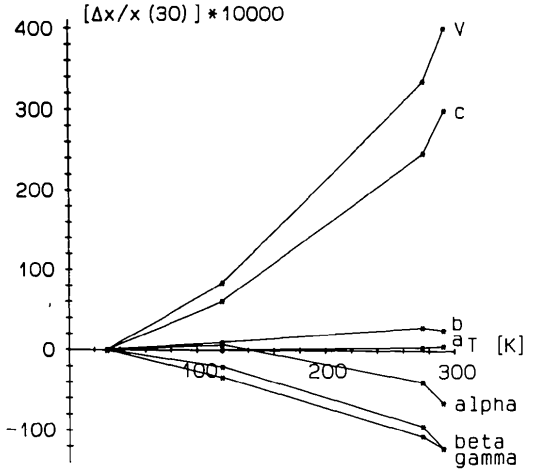

Fig. 4. Relative changes of unit-cell constants $\{[x(T) - x(30\,\mathrm{K})]/x(30\,\mathrm{K})\}$ *versus* temperature. The points for $T = 291$ K have been taken from Jaskólski (1987).

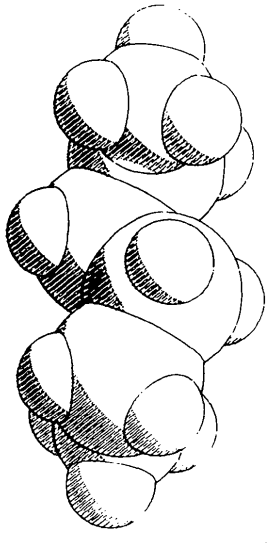

Fig. 5. Space-filling model of cation II*A* illustrating the shape of this g^+tg^- conformer. Cation II*B* has the same, g^-tg^+, conformation and could be generated in the structure by rotating the above II*A* form by 180° along a horizontal axis passing through the center of the diagram.

Table 5. *Bond distances* (Å), *angles* (°) *and torsion angles* (°) *at* 30 K (*first value*), 120 K (*second value*) *and* 275 K (*third value*)

Bond distances have not been corrected for thermal motion and provide therefore a measure of the thermal-motion effects in different components of the crystal structure.

N(11)–C(12)	1·500 (1)	N(21)–C(22)	1·500 (1)
	1·500 (1)		1·497 (2)
	1·496 (2)		1·489 (3)
C(12)–C(13)	1·518 (1)	C(22)–C(23*A*)	1·528 (2)
	1·516 (2)		1·528 (2)
	1·506 (2)		1·535 (3)
C(13)–C(13^{i})	1·531 (2)	C(22)–C(23*B*)*	1·542 (1)
	1·527 (2)		1·542 (1)
	1·519 (4)		1·541 (1)
N(10)–O(11)	1·256 (1)	C(23*A*)–C(23*A*^{ii})	1·531 (2)
	1·255 (1)		1·525 (3)
	1·250 (2)		1·510 (6)
N(10)–O(12)	1·252 (1)	C(23*B*)–C(23*B*^{ii})	1·561 (9)
	1·247 (1)		1·536 (9)
	1·236 (2)		1·53 (1)
N(10)–O(13)	1·265 (1)	N(20)–O(21)	1·263 (1)
	1·259 (1)		1·258 (1)
	1·245 (2)		1·251 (2)
		N(20)–O(22)	1·259 (1)
			1·255 (1)
			1·246 (2)
		N(20)–O(23)	1·249 (1)
			1·244 (1)
			1·227 (2)

N(11)–C(12)–C(13)	110·6 (1)	O(11)–N(10)–O(12)	121·2 (1)
	110·6 (1)		121·3 (1)
	111·3 (1)		121·5 (2)
C(12)–C(13)–C(13^{i})	110·7 (1)	O(11)–N(10)–O(13)	119·2 (1)
	110·7 (1)		119·0 (1)
	111·4 (2)		118·6 (2)
N(21)–C(22)–C(23*A*)	111·4 (1)	O(12)–N(10)–O(13)	119·6 (1)
	111·5 (1)		119·7 (1)
	111·2 (2)		119·9 (2)
N(21)–C(22)–C(23*B*)	109·0 (2)	O(21)–N(20)–O(22)	118·9 (1)
	109·2 (2)		118·8 (1)
	109·2 (3)		118·3 (1)
C(22)–C(23*A*)–C(23*A*^{ii})	112·6 (1)	O(21)–N(20)–O(23)	119·8 (1)
	112·4 (1)		119·7 (1)
	112·2 (2)		119·7 (2)
C(22)–C(23*B*)–C(23*B*^{ii})	110·3 (2)	O(22)–N(20)–O(23)	121·3 (1)
	110·8 (2)		121·5 (1)
	111·0 (3)		122·0 (2)

N(11)–C(12)–C(13)–C(13^{i})	178·9 (1)
	178·8 (1)
	178·5 (2)
N(21)–C(22)–C(23*A*)–C(23*A*^{ii})	−67·5 (1)
	−68·1 (1)
	−70·7 (3)
N(21)–C(22)–C(23*B*)–C(23*B*^{ii})	75·1 (3)
	75·1 (3)
	76·8 (5)

Symmetry codes: (i) $-x, -y, 1-z$; (ii) $1-x, -y, -z$.

* Restrained.

Table 6. *Geometry* (Å, °) *of the* H *bonds at* 30 K

N–H···O	N–H	H···O	N···O	∠N–H···O
N(11)–H(111)···O(11^{i})	0·97 (1)	2·16 (1)	2·964 (1)	139·1 (8)
N(11)–H(112)···O(13^{ii})	0·98 (1)	1·91 (1)	2·891 (1)	173·2 (8)
N(11)–H(113)···O(21^{ii})	0·98 (1)	2·38 (1)	3·076 (1)	127·8 (8)
N(11)–H(113)···O(23^{ii})	0·98 (1)	2·08 (1)	3·052 (1)	171·2 (7)
N(21)–H(211)···O(12)	0·98 (1)	2·36 (2)	3·084 (1)	130·9 (8)
N(21)–H(212)···O(22^{iii})	0·98 (1)	1·84 (1)	2·811 (1)	174·0 (9)
N(21)–H(213)···O(21^{iv})	0·98 (1)	1·88 (1)	2·854 (1)	172·8 (8)
N(21)–H(213)···O(22^{iv})	0·98 (1)	2·31 (1)	2·992 (1)	125·8 (8)

Symmetry codes: (i) $1-x, 1-y, 1-z$; (ii) $x, y-1, z$; (iii) $-x, -y, 1-z$; (iv) $-x, 1-y, 1-z$.

We wish to thank Mr Hilding Karlsson, Institute of Chemistry, University of Uppsala, for technical assistance during the measurements. This work was partly supported by project RPBP 01·6 (Polish Academy of Sciences).

References

BARTOSZAK, E. & JASKÓLSKI, M. (1988). *Acta Cryst.* Submitted.
CHANDRASEKHAR, K. & PATTABHI, V. (1980). *Acta Cryst.* B**36**, 2486–2488.
FURBERG, S. & SOLBAKK, J. (1972). *Acta Chem. Scand.* **26**, 2855–2862.
International Tables for X-ray Crystallography (1974). Vol. IV. Birmingham: Kynoch Press. (Present distributor Kluwer Academic Publishers, Dordrecht.)
JASKÓLSKI, M. (1982). *Collected Abstracts of the Fourth Symposium on Organic Crystal Chemistry*, Poznań, September 1982, edited by Z. KAŁUSKI, pp. 70–71. Poznań: UAM.
JASKÓLSKI, M. (1987). *Acta Cryst.* C**43**, 1761–1763.
JASKÓLSKI, M., ALEJSKA, M. & WIEWIÓROWSKI, M. (1986). *J. Crystallogr. Spectrosc. Res.* **16**, 31–39.
JOHNSON, C. K. (1976). *ORTEP*II. Report ORNL-5138. Oak Ridge National Laboratory, Tennessee, USA.
LEHMANN, M. S. & LARSEN, F. K. (1974). *Acta Cryst.* A**30**, 580–584.
LUNDGREN, J.-O. (1982). *Crystallographic Computer Programs.* Report UUIC-B13-4-05. Institute of Chemistry, Univ. of Uppsala, Sweden.
MOTHERWELL, W. D. S. & CLEGG, W. (1978). *PLUTO.* Program for plotting molecular and crystal structures. Univ. of Cambridge, England.
SHELDRICK, G. M. (1976). *SHELX*76. Program for crystal structure determination. Univ. of Cambridge, England.
TAKUSAGAWA, F. & KOETZLE, T. F. (1978). *Acta Cryst.* B**34**, 1910–1915.
TAKUSAGAWA, F. & KOETZLE, T. F. (1979). *Acta Cryst.* B**35**, 867–877.
WOO, N. H., SEEMAN, N. C. & RICH, A. (1979). *Biopolymers*, **18**, 539–552.

Acta Cryst. (1989). B**45**, 85–92

Structure Determination of Mengo Virus

BY MING LUO,* GERRIT VRIEND,† GREG KAMER AND MICHAEL G. ROSSMANN

Department of Biological Sciences, Purdue University, West Lafayette, Indiana 47907, *USA*

(*Received* 9 *May* 1988; *accepted* 16 *September* 1988)

Abstract

The structure of Mengo virus was determined to 3·0 Å resolution using human rhinovirus 14 as an initial phasing model at 8·0 Å resolution. Oscillation diffraction photographs were collected at the Cornell High Energy Synchrotron Source using orthorhombic Mengo virus crystals. The crystal space group was $P2_12_12_1$, $a = 441{\cdot}4$, $b = 427{\cdot}3$ and $c = 421{\cdot}9$ Å, with one icosahedral particle per asymmetric unit, giving 60-fold noncrystallographic redundancy. The orientations of the four viral particles in the unit cell were determined with a rotation function. Their positions relative to the crystallographic symmetry axes were found by a combination of Patterson-function analysis and a subsequent R-factor search using human rhinovirus 14 atomic coordinates as a model. The initial phases to 8·0 Å resolution were then computed by placing human rhinovirus 14 particles in the orientations and positions of Mengo virus particles. These phases were improved by ten cycles of real-space molecular replacement averaging. Phases between 8·0 and 3·0 Å resolution were obtained by molecular replacement phase extension. One or two reciprocal-space lattice points were used for each extension followed by two cycles of averaging.

Introduction

Mengo virus is a small icosahedral RNA animal virus with a molecular weight of $8{\cdot}5 \times 10^6$. About 30% of its mass is RNA. It belongs to the family of picornaviruses (Rueckert, 1986) and the genus cardiovirus. There are 60 copies of each of four different viral proteins (VP1, VP2, VP3 and VP4) in its coat. The course of the structure determination was similar to that of human rhinovirus 14 (HRV14) (Rossmann, Arnold, Erickson, Frankenberger, Griffith, Hecht, Johnson, Kamer, Luo, Mosser, Rueckert, Sherry & Vriend, 1985) and poliovirus (Hogle, Chow & Filman, 1985), although the structure itself is substantially different. VP1, VP2 and VP3 of Mengo virus have 12, 30 and 23% identical amino acids to HRV14; there are 47, 22 and 7 amino acids of Mengo virus that are insertions with respect to HRV14 and 62, 28 and 13 amino acids of HRV14 that are insertions with respect to Mengo virus, respectively. The Mengo virus structure has been

* Present address: Center for Macromolecular Crystallography, Department of Microbiology, University Station, University of Alabama, Birmingham, Alabama 35294, USA.
† Present address: Department of Structural Chemistry, University of Groningen, Nijenborgh 16, 9747 AG Groningen, The Netherlands.

0108-7681/89/010085-08$03.00